Journal of Sound and Vibration (1997) **200**(4), 441–465

THE USE OF "ECTOPLASM" TO PREDICT RADIATION AND TRANSMISSION LOSS OF A HOLED PLATE IN A CAVITY

O. Beslin†

Laboratoire des Sciences de l'Habitat, Département Génie Civil et Batiment—CNRS URA D 1652, *Ecole Nationale des Travaux Publics de l'Etat, Rue Maurice Audin*, 69518 *Vaulx-en-velin cedex, France*

AND

J. L. Guyader

Laboratoire Vibrations-Acoustique, Batiment 303, *Institut National des Sciences Appliquées de Lyon*, 20 *Avenue Albert Einstein*, 69621 *Villeurbanne cedex, France*

(*Received* 15 *November* 1994, *and in final form* 24 *July* 1996)

The purpose of this paper is to extend the use of "ectoplasm" to a vibro-acoustic problem. The notion of ectoplasm had been presented in a previous paper treating the prediction of natural mode shapes of plates with holes of any shape. It was shown that a structure originally defined on a complex domain can be prolonged by an insubstantial mechanical medium (ectoplasm) in order to be defined on a canonical domain. Then, a semi-analytical calculus can be used. Ectoplasm characteristics must not perturb the structure behaviour, but must cover round-off errors of the computer. Here it is shown that such a compromise is still valid when the structure is coupled to a fluid. A holed plate is considered, separating a rectangular cavity in two parts. An integral formulation is used to describe the pressure field. The cavity Green function is expanded on twice indexed functions, implicitly allowing to take into account the pressure field discontinuity, and save running time. The plate is considered as a heterogeneous plate containing ectoplasm, defined on all the sections of the cavity and a variational formulation is used. Radiation and transmission loss of a holed plate is discussed and compared with the case of a full plate. The case of the non-baffled free plate is also presented. The method is validated by comparison with experimental data.

1. INTRODUCTION

Holed plates are often used in engineering. Sometimes, holes are intentionally designed by acousticians in order to improve absorbent panels properties, and in many other cases, holes are present in structures (like sound enclosures) for non-acoustical reasons such as venting, saving weight, for accessibility or visual control of the enclosed machine, etc. Sometimes the holed structure itself is responsible for structure-borne sound. In such cases, optimisation of sizes and positions of the holes could probably be found in many cases in order to minimise radiated noise. It then necessitates parametric studies utilising predicting tools. However, the prediction of transmission loss or radiated power is difficult as holed plates do not have canonical geometries. Classical results and known tendencies of canonical structures in the literature (rectangular, circular, infinite, baffled

†Present address: Groupe d'Acoustique de l'Université de Sherbrooke, Sherbrooke, QC J1K 2R1, Canada.

0022–460X/97/090441 + 25 $25.00/0/sv960711

plates, cylindrical shells...) cannot be used, as singular effects occur such as acoustical short circuits that are difficult to quantify.

Predicting the behaviour of fluid loaded holed plates presents two main difficulties: firstly, natural modes shapes of holed plates must be known (including high order modes). Secondly, the presence of holes requires that the classical ''baffle condition'' used when predicting structure radiation must be abandoned. Then, treating a non-baffled problem, a double layer potential density must be considered, leading to the classical high singularity of the Green kernel derivative.

There are two kinds of holed plates: plates with an array of small holes and plates with one or a few holes (having any sort of size and shape). Plates with an array of holes (or slits) have been treated in the literature by regarding their absorption properties. Salikuddin has shown experimentally [1] and theoretically [2] that such perforated plates can be used as anechoic terminations in ducts when the incident wave is of high pulse intensity. It was concluded that the absorption is due to non-linear propagation effects, and that its magnitude depends on the porosity of the termination and the intensity of propagating sound waves (vortex formation, induced by the holes, acts on the absorption mechanism). Dowling [3] has studied a screen perforated by a regular array of parallel slits with a mean bias flow through the slits. He has shown that the interaction between an incident sound wave and the mean bias flow converts acoustical energy into non-radiative unsteady vortical motion, leading to a linear mechanism of sound absorption.

Radiation of plates with an array of small holes has been experimentally studied by Pierri [4]; it was concluded that the radiation of holed plates decreases as the ''free area'' (total holes surface) of the plate increases. However, for plates having small free area, differences compared with a full plate vanish for high frequencies. Plates with an array of small holes have also interesting properties when used in a double-leaf panel. Classically, double-leaf panels have a better transmission loss than simple-leaf panels, except at the resonant frequency ''mass-stiffness-mass'' of the double-leaf structure where the tendecy is reversed. Atwal and Crocker [5] have experimentally shown that the transmission loss can be improved at this resonant frequency when perforating one of the leaves, finally leading to a better global transmission loss than a classical double-leaf panel. The effect of perforations on fixed single-leaf and double-leaf panels also has been treated by Ffowcs Williams [6] and Leppington and Levine [7]; similar tendencies were observed with honeycomb sandwich panels. Transmission loss can be improved by perforating one of the leaves so as to link honeycomb cells to the exterior fluid. Leppington [8] has proposed a theoretical model to express the effective boundary conditions for a perforated elastic sandwich panel in a compressible fluid. The compound panel is shown to be acoustically equivalent to that of a hypothetical surface with different normal velocities on either side.

Plates with one or a few holes (of medium or large dimensions) have been reported less in the literature. Pan [9] has used a perforated plate as acoustical actuator for active control, but he considered only the first plate mode that was assumed to be the same as full plate mode. Mechel [10] had studied acoustical transmission through a small hole in a rigid wall by using an electro-mechanical analogy. Murashi [11] had experimentally discussed the influence on transmission loss of a hole positioned in a wall separating two rooms. Ouellet [12] predicted the sound field in a rectangular cavity enclosing a thin limp panel. The panel was acoustically introduced as a double layer potential density. This last formulation is close to the one presented in this paper, but improvements are proposed in order to reach better convergence and the panel is considered as a plate having modes. No paper treating perforated panels, having any hole shape, taking into account vibratory modes and full coupling with the fluid medium, has been found in the literature.

The first contribution of this study is to consider holed plates with their own modal behaviour. This implies the use of a holed plate operator. A representation of such an operator on a functional basis was proposed in a previous paper [13]. Then, to avoid ill-conditioning of mass and stiffness matrices, a new notion of "ectoplasm" was developed. Ectoplasm is an insubstantial mechanical medium having no influence on the plate motion but having some effect in terms of numerical round-off errors. The second contribution is the extension of the use of ectoplasm to a vibro-acoustic problem and shows that ectoplasm can remain negligible compared with light fluid medium such as air. It permits a plate with a complex arrangement of holes to be treated as a heterogeneous structure defined on a canonical domain. Then, a semi-analytical formulation can be used and many simplifications occur in the calculations. A third contribution is to remove the double layer potential singularity by considering the holed plate in a cavity, and using an expansion of the cavity Green function which implicitly takes into account the pressure jump across the plate. Moreover, the Green function expansion is defined by double index basis functions instead of the classical three index functions, which saves running time.

The paper is organised as follows. The acoustical part of the problem is treated using an integral formulation. The unknown pressure jump across the plate is described as an expansion of cosine functions. The fluid loaded holed plate motion is taken into account using a holed plate operator developed in a previous paper [13], linking the pressure jump and the plate displacement, which is the second unknown of the problem (expanded in sine functions). The second equation for coupling plate and cavity is the continuity of velocities on the plate surface. Then, the convergence of the method and the negligibility of the ectoplasm compared with the fluid medium characteristic impedance are studied and criteria are found. The influence of a hole on plate radiation and transmission loss is discussed, and the numerical code is validated by comparing with experimental results. Finally a simulation of a non-baffled free plate is presented as an extreme case of a holed plate than can be treated using ectoplasm.

2. BASIC THEORY

2.1. DESCRIPTION OF THE PROBLEM

A parallelepipedic rigid walled cavity of dimensions: $a \times b \times l$ (Figure 1) is considered. A plate of dimensions $a \times b$ containing cut-outs is placed perpendicularly to the z-axis,

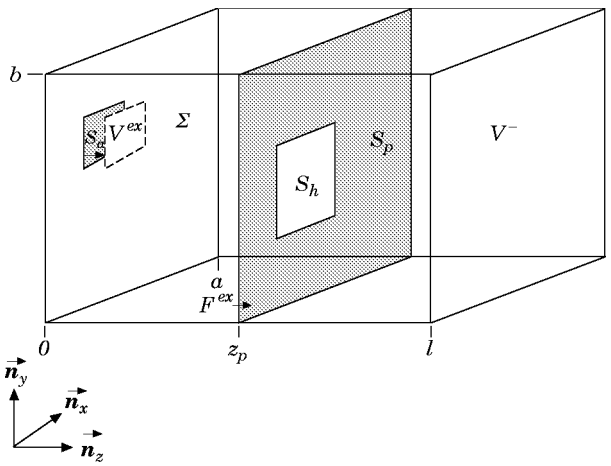

Figure 1. Typical problem.

at $z = z_p$. The surface of the total plate (including the holes) is denoted by S. Two ways of harmonic excitation at angular frequency ω are considered. A mechanical excitation of the holed plate at point $M_F(x_F, y_F)$:

$$F^{ex}(x, y, t) = \bar{F}^{ex}\delta(x - x_F)\delta(y - y_F)\,\mathrm{e}^{\mathrm{j}\omega t}, \quad (x, y)\in S, \tag{1}$$

and an acoustical excitation, introduced as a vibrating piston of velocity V^{ex} and surface S_a, lying on a wall of the cavity at $z = 0$:

$$V^{ex}(x, y, t) = \bar{V}^{ex}\,\mathrm{e}^{\mathrm{j}\omega t}, \quad (x, y)\in S_a. \tag{2}$$

The first type of excitation allows one to study the acoustical radiation of a holed plate, while the second type can be used to predict the transmission loss of a holed plate. The interior volume of the parallelepiped is defined as V^- and the walls surface Σ. Damping phenomena in the plate (respectively cavity) are taken into account by the use of an imaginary part of Young modulus (respectively acoustical wave number):

$$E\to E(1 - \mathrm{j}\eta_s), \qquad k^2\to k^2(1 - \mathrm{j}\eta_a). \tag{3, 4}$$

2.2. INTEGRAL FORMULATION FOR THE PRESSURE IN THE CAVITY

The pressure field in the cavity $p(M)$ can be considered as a single and double layer potential; the vibrating surface S_a acting as a layer of monopole sources, and the plate acting as a layer of dipole sources (continuity of velocity and discontinuity of pressure across the plate). The density of the simple layer is imposed (as the acoustical excitation source), but the density of the double layer is an unknown of the problem. It represents the pressure jump across the plate, and will be noted $\bar{P}(M_0)$, where $M_0(x_0, y_0, z_p)$ is a point lying on the surface S:

$$\bar{P}(M_0) = \lim_{\varepsilon\to 0^+}\{p(x_0, y_0, z_p + \varepsilon) - p(x_0, y_0, z_p - \varepsilon)\}, \qquad (x_0, y_0)\in[0, a]\times[0, b]. \tag{5}$$

2.2.1. *Helmholtz-Huygens integral*

The pressue field must satisfy the following non-homogeneous Helmholtz equation and boundary conditions:

$$(\Delta + k^2(1 - \mathrm{j}\eta_a))p(M) = -(\mathrm{d}/\mathrm{d}z)(\bar{P}(M_0)\delta(M, M_0)), \qquad M\in V^-, \quad M_0\in S. \tag{6}$$

$$\vec{\mathbf{V}}(p(M))\circ\vec{\mathbf{n}} = 0, \qquad M\in\Sigma; \qquad \vec{\mathbf{V}}(p(M))\circ\vec{\mathbf{n}} = \mathrm{j}kZ_0\bar{V}^{ex}, \qquad M\in S_a, \tag{7, 8}$$

where $\vec{\mathbf{n}}$ is the normal vector relative to the Σ or S_a surface, pointing toward the exterior of the cavity, k is the wave number and Z_0 the characteristic impedance of the fluid:

$$k = \omega/c_0, \qquad Z_0 = \rho_f c_0; \tag{9, 10}$$

c_0 and ρ_f are the celerity of sound and the fluid density, respectively.

Using integral formulation (reference [14], p. 262, reference [15], p. 181), the pressure field, solution of equations (6–8), can be expressed as

$$p(M) = \int_{S_a}\mathrm{j}kZ_0\bar{V}^{ex}G_k(M, M_0)\,\mathrm{d}S_0 + \int_S \bar{P}(M_0)\vec{\mathbf{V}}_{M_0}(G_k(M, M_0))\circ\vec{\mathbf{n}}_z\,\mathrm{d}S_0, \tag{11}$$

where $G_k(M, M_0)$ is a Green function of the problem such that

$$(\Delta_M + k^2(1 - j\eta_a))G_k(M, M_0) = -\delta(M, M_0), \qquad \forall M \in V^-, \tag{12}$$

$$\vec{\nabla}_M(G_k(M, M_0)) \circ \hat{\mathbf{n}} = 0, \qquad \forall M \in \Sigma \cup S_a. \tag{13}$$

2.2.2. *The Green function*

A classical way to express the Green function satisfying equations (12, 13), is to expand it in terms of cavity modes:

$$G_k(M, M_0) = \sum_{n,p,q \text{ integers} \geqslant 0} g_{npq} \cos(n\pi x/a) \cos(p\pi y/b) \cos(q\pi z/l)$$

$$\times \cos(n\pi x_0/a) \cos(p\pi y_0/b) \cos(q\pi z_0/l). \tag{14}$$

This method leads to two difficulties for the present application: (1) coefficients g_{npq} depend on three indices. This leads to large matrices. (2) It is a well known property of Fourier series that when they approximate discontinuous functions, the term by term derivative of the series expansion is different from the true derivative of the function [16]. This is the case here as the plate generates a pressure jump. However, Ouellet [12] has used this method; it was needed then to introduce supplementary unknown coefficients representing the expansion of the pressure gradient. This technique leads to large matrix sizes as well.

Another way to express the Green function satisfying equations (12, 13) was proposed by Bruneau (reference [14] p. 514): the Green function can be expanded on a double indexed ortho-normal basis $\{\psi_{rs}\}$ satisfying Neumann boundary conditions:

$$G_k(M, M_0) = \sum_{(r,s) \text{ integers} \geqslant 0} g_{rs}(z, z_0)\psi_{rs}(x, y)\psi_{rs}(x_0, y_0). \tag{15}$$

The $g_{rs}(z, z_0)$ are functions having discontinuous slope at $z = z_0$. This allows us to take into account the pressure jump along the z-axis when the derivative of the Green function along the z-axis is used. In such a way, problems of Fourier series derivatives are removed and two indices are needed instead of three, leading to smaller matrices than the classical approach. This last method was retained to treat the present problem.

A $\{\psi_{rs}\}$ ortho-normal basis set satisfying Neumann boundary condition is

$$\psi_{rs}(x, y) = \sqrt{(2 - \delta_{0r})(2 - \delta_{0s})/ab} \cos(r\pi x/a) \cos(s\pi y/b), \tag{16}$$

where δ_{0r} is the Kronecker's symbol:

$$\delta_{ij} = \begin{cases} 0 & \text{if} \quad i \neq j \\ 1 & \text{if} \quad i = j \end{cases}. \tag{17}$$

The $\{\psi_{rs}\}$ functions satisfy the ortho-normal relation

$$\int_S \psi_{rs}(x, y)\psi_{r's'}(x, y)\, \mathrm{d}S = \delta_{rr'}\delta_{ss'}. \tag{18}$$

Substituting the expression (15) of the Green function into the Helmholtz equations (12, 13) and using the orthogonality property (18) demonstrates that each $g_{rs}(z, z_0)$ functions must be such that

$$\partial^2 g_{rs}(z, z_0)/\partial z^2 + k_{zrs}^2 g_{rs}(z, z_0) = -\delta(z - z_0), \qquad \forall z \in [0, l], \tag{19}$$

$$\partial g_{rs}(z, z_0)/\partial z|_{z=0} = 0; \qquad \partial g_{rs}(z, z_0)/\partial z|_{z=l} = 0, \tag{20, 21}$$

where k_{zrs} is the z-axis component of the wave vector, such that

$$k_{zrs}^2 + k_{rs}^2 = k^2(1 - \mathrm{j}\eta_a) \tag{22}$$

and k_{rs} is the projection of the wave vector on the x-y plane:

$$k_{rs}^2 = (r\pi/a)^2 + (s\pi/b)^2. \tag{23}$$

The wave number k_{zrs} can be expressed in the form

$$k_{zrs} = \tilde{k}_{zrs} - \mathrm{j}\Gamma_{rs}, \tag{24}$$

where $\tilde{k}_{zrs}$ and Γ_{rs} are real and positive quantities given by

$$\tilde{k}_{zrs} = k/\sqrt{2}\sqrt{\sqrt{[(k_{rs}/k)^2 - 1]^2 + \eta_a^2} - [(k_{rs}/k)^2 - 1]}, \tag{25}$$

$$\Gamma_{rs} = k/\sqrt{2}\sqrt{\sqrt{[(k_{rs}/k)^2 - 1]^2 + \eta_a^2} + [(k_{rs}/k)^2 - 1]}. \tag{26}$$

$g_{rs}(z, z_0)$ is a mono-dimensional Green function that can be expressed as

$$g_{rs}(z, z_0) = -\cos(k_{zrs}(l - z_0))\cos(k_{zrs}z)/k_{zrs}\sin(k_{zrs}l), \qquad \forall z \in [0, z_0[, \tag{27}$$

$$g_{rs}(z, z_0) = -\cos(k_{zrs}z_0)\cos(k_{zrs}(z - l))/k_{zrs}\sin(k_{zrs}l), \qquad \forall z \in]z_0, l]. \tag{28}$$

$g_{rs}(z, z_0)$ is a continuous function in $[0, l]$. However, as mentioned previously, $g_{rs}(z, z_0)$ has a slope discontinuity at $z = z_0$. It can be noted that, for high order (r, s) indices (where $k_{rs} \gg k$) the real part of k_{zrs} tends toward zero, and the imaginary part of k_{zrs} tends toward $-k_{rs}$ (a large negative value), leading to strongly evanescent waves. This insures the good convergence of the method.

2.2.3. *The pressure field*

Substituting the expressions (27,28) of the Green function into the integral formulation of the pressure in the cavity (11), an expansion of the pressure field on the ψ_{rs} functions is finally obtained as follows:

$$p(M) = \sum_{r,s} [\bar{P}_{rs}(\alpha_{rs}(z) + \mathrm{U}(z - z_p)) + \bar{V}_{rs}^{ex} Z_0 \beta_{rs}(z)]\psi_{rs}(x, y), \qquad \forall z \in [0, l]. \tag{29}$$

$\mathrm{U}(z)$ is the Heaviside function:

$$\begin{cases} \mathrm{U}(z) = 0, & \text{if} \quad z < 0, \\ \mathrm{U}(z) = 1, & \text{if} \quad z > 0. \end{cases} \tag{30}$$

$\alpha_{rs}(z)$ and $\beta_{rs}(z)$ and their first derivatives are continuous functions in the domain $[0, l]$:

$$\alpha_{rs}(z) = -\sin(k_{zrs}(l - z_p))\cos(k_{krs}z)/\sin(k_{zrs}l), \qquad \forall z \in [0, z_0], \tag{31}$$

$$\alpha_{rs}(z) = \sin(k_{zrs}z_p)\cos(k_{krs}(l-z))/\sin(k_{zrs}l) - 1, \qquad \forall z \in [z_0, l], \tag{32}$$

$$\beta_{rs}(z) = -jk\cos(k_{zrs}(l-z))/k_{zrs}\sin(k_{zrs}l), \qquad \forall z \in [0, l]. \tag{33}$$

$\bar{V}_{rs}^{ex}$ is the projection of the velocity of the vibrating surface S_a in $\{\psi_{rs}\}$ basis functions:

$$\bar{V}_{rs}^{ex} = \bar{V}^{ex}\int_{S_a}\psi_{rs}(x, y)\,\mathrm{d}S. \tag{34}$$

$\bar{P}_{rs}$ are unknown expansion coefficients of the pressure jump in $\{\psi_{rs}\}$ basis functions:

$$\bar{P}_{rs} = \int_S \bar{P}(x, y)\psi_{rs}(x, y)\,\mathrm{d}S. \tag{35}$$

The presence of the Heaviside function in the pressure field expression (29) takes into account the pressure field discontinuity. It can be seen that using this expression of the pressure field in the definition (5) of the pressure jump, it can be described because $\alpha_{rs}(z)$ and $\beta_{rs}(z)$ are continuous:

$$\bar{P}(x_0, y_0) = \sum_{r,s}\bar{P}_{rs}\psi_{rs}(x_0, y_0). \tag{36}$$

This is consistent with the above expression (35) of $\bar{P}_{rs}$.

2.3. SIMULATING THE HOLED PLATE

In the above acoustical part of the formulation, the presence of the plate is taken into account by the pressure jump function (36). The pressure jump acts on the plate as a loading force density that adds to the mechanical exiting force. For a harmonic motion, the plate displacement (respectively the loading force density) has the form $W(x, y, t) = \bar{W}(x, y)\,\mathrm{e}^{\mathrm{j}\omega t}$ (respectively $f(x, y, t) = \bar{f}(x, y)\,\mathrm{e}^{\mathrm{j}\omega t}$). The holed plate displacement field $\bar{W}(x, y)$ and the loading force density $\bar{f}(x, y)$ can be linked by a holed plate operator Z that takes into account the holed plate mechanical characteristics:

$$Z(\bar{W}(x, y)) = \bar{f}(x, y). \tag{37}$$

It was shown in a previous paper [13] that a representation of the Z operator in the modal basis of a full plate can be obtained. Such a formulation allows one to calculate high order holed plate modes at small numerical cost but leads to a non-unique solution for the plate displacement $W(x, y)$ and thus, to ill-conditioned mass and stiffness matrices. It was shown that, to remove the non-uniqueness problem and avoid ill-conditioned matrices, the holes must be considered as a mechanical medium having negligible characteristics compared to the plate but not negligible in terms of the round-off errors of the computer ε ($\approx 10^{-15}$). This insubstantial mechanical medium was named "ectoplasm".

2.3.1. *Using ectoplasm*

The holed plate is supposed to be simply supported on its exterior contour Γ_p, and free on the holes contour Γ_h. The plate motion must then satisfy two types of boundary conditions:

$$\text{Natural boundary conditions: } \begin{cases} \textit{Bending moment} = 0, & \text{for} \quad (x, y) \in \Gamma_h \cup \Gamma_p, \\ \textit{Shearing force} = 0, & \text{for} \quad (x, y) \in \Gamma_h. \end{cases} \tag{38}$$

$$\text{Essential boundary conditions } W(x, y, t) = 0 \quad \text{for} \quad (x, y) \in \Gamma_p. \tag{39}$$

The plate area (excluding the hole) is denoted S_p and the holes area is denoted S_h (such that $S = S_p \cup S_h$). On the S_p area, the classical mechanical parameters of the Love-Kirchhoff theory are used: ρ_s mass per unit area, E Young modulus, v Poisson ratio, h plate thickness, η structural damping coefficient,

$$D = Eh^3(1 + \mathrm{j}\eta)/12(1 - v^2)\text{: bending stiffness.} \tag{40}$$

As mentioned previously, in order to avoid ill-conditioned problems, the real holed plate (defined by the S_p area) must be replaced by a heterogeneous plate defined by the S area. The heterogeneous plate must have the same mechanical characteristics as the holed plate in the S_p area, and have insubstantial ectoplasmic characteristics (ρ_{ect}, D_{ect}) in the S_h area:

$$\rho(x, y) = \rho_s + \rho_{ect}, \quad \text{for} \quad (x, y) \in S_p; \qquad \rho(x, y) = \rho_{ect}; \quad \text{for} \quad (x, y) \in S_h; \tag{41, 42}$$

$$D(x, y) = D + D_{ect}; \quad \text{for} \quad (x, y) \in S_p; \qquad D(x, y) = D_{ect}, \quad \text{for} \quad (x, y) \in S_h; \tag{43, 44}$$

$$\varepsilon < \rho_{ect}/\rho_s \ll 1, \qquad \varepsilon < D_{ect}/D \ll 1, \tag{45, 46}$$

where ε is the order of magnitude of the computer round-off error ($\sim 10^{-15}$ when using double precision).

2.3.2. *The holed plate operator*

The plate displacement $W(x, y, t)$ and the loading force density $f(x, y, t)$ can be expressed as

$$W(x, y, t) = \bar{W}(x, y)\, \mathrm{e}^{\mathrm{j}\omega t}, \qquad f(x, y, t) = \bar{f}(x, y)\, \mathrm{e}^{\mathrm{j}\omega t}, \qquad (x, y) \in S. \tag{47, 48}$$

In order to obtain a representation of the Z operator on a functional basis $\{\phi_{nm}\}$, the plate displacement is expanded on the modal basis $\{\phi_{nm}\}$ of the full plate (before cutting it out) satisfying the essential boundary conditions (39):

$$\bar{W}(x, y) = \sum_{n,m \text{ integers} > 0} \bar{W}_{nm}\phi_{nm}(x, y), \qquad \phi_{nm}(x, y) = \sqrt{(4/ab)}\, \sin(n\pi x/a)\, \sin(m\pi y/b) \tag{49, 50}$$

The Hamilton functional of the plate is given by

$$H(t_1, t_2) = \int_{t_1}^{t_2} \int_S (\mathbf{T}(W(x, y, t)) - \mathbf{U}(W(x, y, t)) + f(x, y, t)W(x, y, t))\, \mathrm{d}S\, \mathrm{d}t. \tag{51}$$

T and **U** are, respectively, the kinetic and potential energy density:

$$\mathbf{T}(W(x, y, t)) = (\rho(x, y)/2)(\partial W(x, y, t)/\partial t)^2, \tag{52}$$

$$\mathbf{U}(W(x, y, t)) = (D(x, y)/2)[(\partial^2 W(x, y, t)/\partial x^2)^2 + (\partial^2 W(x, y, t)/\partial y^2)^2 + 2\nu\, \partial^2 W(x, y, t)/\partial x^2\, \partial^2 W(x, y, t)/\partial y^2 + 2(1-\nu)(\partial^2 W(x, y, t)/\partial x\, \partial y)^2]. \quad (53)$$

When the Hamilton function (51) is at extremum versus the $\overline{W}_{nm}$ coefficients, the following linear system is obtained:

$$[Z_{pqnm}] \cdot \{\overline{W}_{nm}\} = \{\overline{f}_{pq}\}, \qquad \overline{f}_{pq} = \int_S \phi_{pq}(x, y)\, \overline{f}\,(x, y)\, \mathrm{d}S. \quad (54, 55)$$

The f_{pq} are generalised loading force densities. $[\mathbf{Z_{pqnm}}]$ is the representation of the holed plate operator in the $\{\phi_{nm}\}$ basis functions. It can be expressed using stiffness and mass matrices, as classically done:

$$\{\mathbf{Z_{pqnm}}\} = \{\mathbf{K_{pqnm}}\} - \omega^2\{\mathbf{M_{pqnm}}\}, \quad (56)$$

with

$$K_{pqnm} = \frac{D\pi^4}{a^2b^2}[(b^2/a^2)n^2p^2 + (a^2/b^2)m^2q^2 + \nu(n^2q^2 + p^2m^2)]A_{pqnm} + 2D(1-\nu)\beta_{pqnm} + D_{ect}[(n\pi/a)^2 + (m\pi/b)^2]^2\delta_{np}\delta_{mq}, \quad (57)$$

$$M_{pqnm} = \rho_s A_{pqnm} + \rho_{ect}\delta_{nm}\delta_{pq}, \qquad A_{pqnm} = \int_{S_p} \phi_{pq}(x, y)\phi_{nm}(x, y)\, \mathrm{d}S,$$

$$B_{pqnm} = \int_{S_p} \frac{\partial^2\phi_{pq}(x, y)}{\partial x\, \partial y}\frac{\partial^2\phi_{nm}(x, y)}{\partial x\, \partial y}\, \mathrm{d}S. \quad (58\text{–}60)$$

If there is no hole in the plate, the classical result is found, with diagonal matrices:

$$K_{pqnm} = D[(n\pi/a)^2 + (m\pi/b)^2]^2\delta_{np}\delta_{mq}, \qquad M_{pqnm} = \rho_s\delta_{np}\delta_{mp}. \quad (61, 62)$$

2.4. COUPLING PLATE AND CAVITY

Cavity and plate must be coupled, using two equations describing the fluid loaded plate motion, and the continuity of velocities across the plate. Both equations are established in the following sections.

2.4.1. *Fluid loaded plate motion*

Using the pressure jump expression (36), the total loading force density acting on the plate can be expressed as

$$\overline{f}(x, y) = \overline{F}^{ex}(x, y) - \sum_{r,s} \overline{P}_{rs}\psi_{rs}(x, y). \quad (63)$$

Then, using equation (55), the generalised loading force density is given by

$$\overline{f}_{pq} = \overline{F}^{ex}_{pq} - C_{pqrs}\overline{P}_{rs}, \quad (64)$$

where $\bar{F}_{pq}^{ex}$ are the generalised mechanical driving forces

$$\bar{F}_{pq}^{ex} = \int_S \phi_{pq}(x, y)\bar{F}^{ex}(x, y)\,\mathrm{d}S, \tag{65}$$

$[\mathbf{C_{pqrs}}]$ is a projection matrix (from $\{\psi_{rs}\}$ to $\{\phi_{nm}\}$),

$$C_{pqrs} = \int_S \phi_{pq}(x, y)\psi_{rs}(x, y)\,\mathrm{d}S. \tag{66}$$

Finally, from equations (54) and (64), the fluid-loaded equation of motion is expressed by the following linear system:

$$[\mathbf{Z_{pqnm}}] \cdot \{\bar{W}_{nm}\} = \{\bar{F}_{pq}^{ex}\} - [\mathbf{C_{pqnm}}] \cdot \{\bar{P}_{rs}\}. \tag{67}$$

2.4.2. *Continuity of normal velocities across the plate*

The acoustical velocity $\vec{\mathbf{v}}_a(M)$ at any point $M(x, y, z)$ in the cavity is given by

$$\vec{\mathbf{v}}_a(M) = (\mathrm{j}/kZ_0)\vec{\mathbf{V}}_M(p(M)). \tag{68}$$

The continuity between the plate normal velocity and the acoustical velocity is written as

$$\mathrm{j}\omega\bar{W}(x, y) = \vec{\mathbf{v}}_a(x, y, z_p) \circ \vec{\mathbf{n}}_z, \qquad (x, y) \in S; \tag{69}$$

using the expansion (49) of $\bar{W}(x, y)$ on $\{\phi_{nm}\}$ and expression (29) of the pressure field, the above equation becomes

$$\sum_{n,m\ integers > 0} \bar{W}_{nm}\phi_{nm}(x, y) = \sum_{integers \geqslant 0} (\bar{W}_{rs}^{ex} - Y_{rs}\bar{P}_{rs})\psi_{rs}(x, y), \tag{70}$$

with

$$Y_{rs} = (-1/Z_0\omega k)(\mathrm{d}/\mathrm{d}z)\alpha(z)|_{z=z_p}, \qquad \bar{W}_{rs}^{ex} = (\bar{V}_{rs}^{ex}/\omega k)(\mathrm{d}/\mathrm{d}z)\beta_{rs}(z)|_{z=z_p}. \tag{71, 72}$$

Multiplying equation (70) by $\psi_{tu}(x, y)$ and integrating over S, the continuity of velocities leads finally to the linear system

$$[\mathbf{C^t_{tunm}}] \cdot \{\bar{W}_{nm}\} = \{\bar{W}_{tu}^{ex}\} - [\mathbf{Y_{turs}}] \cdot \{\bar{P}_{rs}\}, \tag{73}$$

where $[\mathbf{C^t_{tunm}}]$ is the transposed matrix of $[\mathbf{C_{pqrs}}]$ defined in equation (66), and $[\mathbf{Y_{turs}}]$ is the matrix of elements:

$$Y_{turs} = Y_{rs}\delta_{tr}\delta_{us}. \tag{74}$$

2.4.3. *Linear system to be solved*

By considering the fluid-loaded plate motion equations (67) and the velocities continuity equations (73), the final system is obtained:

$$\begin{bmatrix} Z_{pqnm} & C_{pqrs} \\ \mathbf{C^t_{tunm}} & Y_{turs} \end{bmatrix} \cdot \begin{Bmatrix} \bar{W}_{nm} \\ \bar{P}_{rs} \end{Bmatrix} = \begin{Bmatrix} \bar{F}_{pq}^{ex} \\ \bar{W}_{tu}^{ex} \end{Bmatrix}. \tag{75}$$

The radiation of a holed plate can then be treated by setting $\bar{W}_{tu}^{ex}$ to zero (no acoustical excitation source), while the transmission loss of a holed plate can be simulated by setting $\bar{F}_{pq}^{ex}$ to zero (no mechanical excitation source).

3. CONVERGENCE OF THE METHOD

Convergence of the method and the negligibility of ectoplasm are discussed in this section. Criteria for the $\{\phi_{nm}\}$ and $\{\psi_{rs}\}$ basis sets selection and ectoplasm characteristics are given.

3.1. SELECTION OF THE BASIS FUNCTIONS

To implement this formulation on a computer code, both sets $\{\phi_{nm}\}$ and $\{\psi_{rs}\}$ must be selected. Selection criteria are discussed in the next section.

3.1.1. *Selection criteria for the uncoupled plate*

Criteria have been established in a previous paper [13] to obtain *in-vacuo* holed plate modes using the $\{\phi_{nm}\}$ basis. A wave number k_{nm}, relative to a ϕ_{nm} basis function is defined by

$$k_{nm}^2 = (n\pi/a)^2 + (m\pi/b)^2. \tag{76}$$

Then the retained $\{\phi_{nm}\}$ set is such that

$$\{\phi_{nm}\} = \{\phi_{nm}, \quad \text{such as} \quad k_{nm}^2 \leqslant k_{max(vacuo)}^2\}, \tag{77}$$

where $k_{max(vacuo)}$ must satisfy two criteria, as follows.

3.1.1.1. Frequency criterion

The flexural wave number at ω is defined

$$\tilde{k_f}(\omega) = \omega/c_f(\omega), \tag{78}$$

where $c_f(\omega)$ is the speed of bending waves at angular frequency ω. Then the first criteria that $k_{max(vacuo)}$ must satisfy is

$$k_{max(vacuo)} \geqslant k_f(\omega). \tag{79}$$

This relation is used in order that plate modes having their resonance frequencies below the driving frequency are retained.

3.2.1.2. Geometrical criterion

By considering l_{min}, a holed plate where the characteristic length, l_{min} is the smallest hole dimension, a minimum wavlength λ_{min} is defined as

$$\lambda_{min} = l_{min}/3. \tag{80}$$

$k_{max(vacuo)}$ must satisfy a second criterion:

$$k_{max(vacuo)} \geqslant 2\pi/\lambda_{min}. \tag{81}$$

This relation is used in order that plate modes of sufficiently small wavelength are retained. This is necessary to localise the holes as far as possible. As often as not, the second criterion includes the first one.

3.1.2. *Selection criteria for the coupled system*

For the coupled system, similar ways of selections are retained: *the mechanical set* $\{\phi_{nm}\}$:

$$\{\phi_{nm}\} = \{\phi_{nm}, \quad \text{such as} \quad k_{nm}^2 \leqslant k_{max(mec)}^2\}, \tag{82}$$

and *the acoustical set* $\{\psi_{rs}\}$:

$$\{\psi_{rs}\} = \{\psi_{rs}, \qquad \text{such as} \qquad k_{rs}^2 \leqslant k_{max(acou)}^2\}. \tag{83}$$

Numerical simulations have demonstrated that for the coupled system, convergence necessitates that $k_{max(mec)}$ must be greater than $k_{max(vacuo)}$. The increasing of the $\{\phi_{nm}\}$ set when treating the coupled system is due to the transfer of the basis between $\{\phi_{nm}\}$ and $\{\psi_{rs}\}$ in both ways:

$$\phi_{pq}(x, y) = \sum_{r,s} C_{pqrs}\psi_{rs}(x, y), \qquad \psi_{tu}(x, y) = \sum_{n,m} C_{tumn}^{t}\,\phi_{nm}(x, y). \tag{84, 85}$$

It can be shown [17] that the expansion of a ϕ_{nm} function (sines) on $\{\psi_{rs}\}$ functions (cosines) converges in a better way than the expansion of a ψ_{rs} function on $\{\phi_{nm}\}$ functions. This leads to a dissymmetry of size between the $\{\phi_{nm}\}$ and the $\{\psi_{rs}\}$ sets that must be retained to converge accurately. Namely, the size of the mechanical sine basis must be greater than the acoustical cosine basis. After several simulations [17] accurate criteria for the coupled problem have been found: $k_{max(mec)}$ and $k_{mac(acou)}$ must be such that

$$k_{max(mec)} \approx 1{\cdot}5k_{max(vacuo)}, \qquad k_{max(acou)} \approx k_{max(vacuo)}. \tag{86, 87}$$

3.2. ACOUSTICAL NEGLIGIBILITY OF ECTOPLASM

The mechanical negligibility of ectoplasm has been studied before [13] and the main results are summarised in Section 2.3.1. In the vibroacoustic problem it must be assured that ectoplasm remains negligible compared with the fluid medium acoustical impedance; namely that the pressure jump generated by the ectoplasm is very small compared to the acoustical pressure. Criteria can be found by considering an infinite plate having ectoplasmic characteristics, submitting to an incident plane wave. Then, the required negligibility of the plate impedance compared to the fluid impedance is written as

$$D_{ect}k^4 \sin^4(\theta) - \rho_{ect}\omega^2 \ll Z_0\omega/\cos(\theta), \tag{88}$$

where θ is the angle of incidence of the plane wave, and k is the wave number of the incident wave: ω/c_0. This last inequality leads to the following criteria for the ectoplasm characteristics. (1) The negligibility of the ectoplasm bending stiffness requires that

$$\varepsilon_D \equiv (D_{ect}/\omega Z_0)k^4 \ll 1. \tag{89}$$

(2) The negligibility of the ectoplasm mass requires that

$$\varepsilon_\rho \equiv \omega\rho_{ect}/Z_0 \ll 1. \tag{90}$$

3.3. NUMERICAL EXAMPLE

An example of numerical resolution is presented in this section in order to show the convergence of the proposed method. Characteristics of the simulated case are the following. The cavity dimensions are $a = 0{\cdot}7$ m, $b = 1{\cdot}0$ m, $l = 2{\cdot}0$ m, $z_p = 0{\cdot}6$ m; the fluid medium characteristics are $\rho_f = 1{\cdot}25$ Kg/m^3, $c_0 = 344{\cdot}8$ ms^{-1}; the plate dimensions are $h = 2$ mm, rectangular hole $0{\cdot}25$ m $\times$ $0{\cdot}30$ m, centred at ($0{\cdot}325$, $0{\cdot}5$); the plate characteristics are $\rho_s = 15{\cdot}6$ Kg/m^2, $E = 2{\cdot}0 \times 10^{11}$ Pa, $v = 0{\cdot}3$, $(\rho_{ect}/\rho_s) = (D_{ect}/D_s) = 10^{-13}$; the acoustical excitation acts on a square surface $0{\cdot}1$ m $\times$ $0{\cdot}1$ m, centred at ($0{\cdot}51$, $0{\cdot}27$), (in the $z = 0$ plane), vibrating at 200 Hz. For cavity and plate damping see Table 1.

TABLE 1

Acoustical and mechanical damping

Frequency range (Hz)	12·5–25	25–50	50–100	100–200	200–400	400–800	800–1600
Acoustical damping: η_a	0·1	0·05	0·015	0·013	0·011	0·06	0·04
Mechanical damping: η_s	0·1	0·017	0·015	0·012	0·013	0·013	0·012

3.3.1. *Pressure in the cavity*

The pressure is calculated at two points in the cavity. They are both on an axis parallel to the z-axis and passing through the centre of the hole: (1) point $M_1(0{\cdot}325, 0{\cdot}5, 0{\cdot}55)$ is situated in the part $z < z_p$ of the cavity (close to the hole), (2) point $M_2(0{\cdot}325, 0{\cdot}5, 1{\cdot}5)$ is situated in the part $z > z_p$ of the cavity (far from the hole). A transfer function (dB) between the pressure at point M and acoustical source velocity is defined by

$$L_p(M) = 10^* \log_{10}\left(\int_0^T p^2(M, t)\,\mathrm{d}t \Big/ \int_0^T V^{ex^2}(t)\,\mathrm{d}t\right), \qquad T = 2\pi/\omega. \tag{91}$$

In Figure 2, L_p is plotted for the two points M_1 and M_2. For each point, two curves are plotted, the solid lines represent L_p versus the number of basis functions ϕ_{nm}, while the number of basis functions ψ_{rs} is set to 415. The dashed lines represent L_p versus the number of basis functions ψ_{rs}, while the number of basis functions ϕ_{nm} is set to 841. It can be seen in Figure 2 that convergence is easier with the $\{\psi_{rs}\}$ basis than with the $\{\phi_{nm}\}$ basis for both points M_1 and M_2. This is due to the dissymmetry of the basis transfer as explained in Section 3.1.2. Convergence begins to be reached when using 841 mechanical basis functions ($k_{max(mec)} = 168\ \mathrm{m}^{-1}$) and 415 acoustical basis functions ($k_{max(acou)} = 112\ \mathrm{m}^{-1}$). The smallest dimension of the hole is $l_{min} = 0{\cdot}15$ m. Using the minimum wavelength criteria of

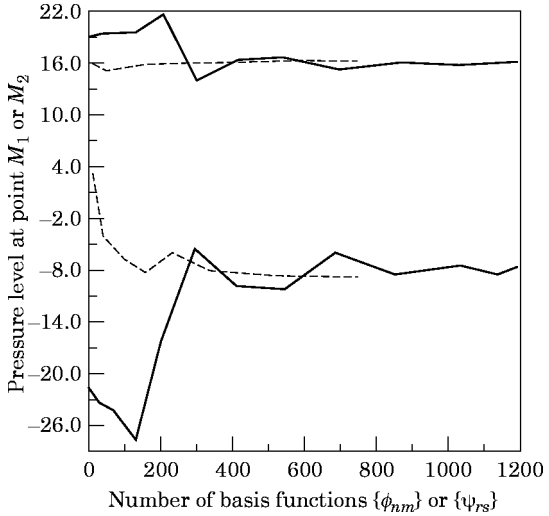

Figure 2. Convergences: ——, number of $\{\psi_{rs}\}$ basis functions is set to 415 and convergence is studied versus the number of $\{\phi_{nm}\}$ basis functions; ——, number of $\{\phi_{nm}\}$ basis functions is set to 841 and convergence is studied versus the number of $\{\psi_{rs}\}$ basis functions. Upper curves, M_1; Lower curves, M_2.

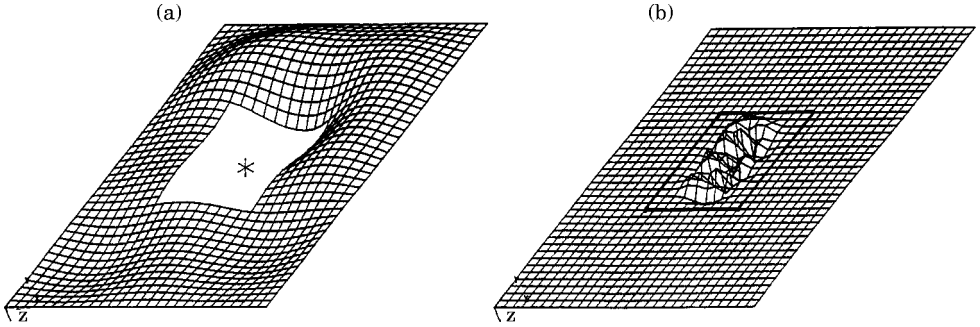

Figure 3. Real part of the plate normal velocity: (a) holed plate surface, (b) domain S including hole area.

section 3.1.1 leads to ($k_{max(mec)} = 188\ \mathrm{m}^{-1}$) and ($k_{max(acou)} = 127\ \mathrm{m}^{-1}$). So, for this case, it can be seen that criteria (86) and (87) are sufficient conditions for accurate convergence. The acoustical negligibility of ectoplasm is verified regarding criteria (89) and (90): numerical application of the stiffness negligibility term leads to $\varepsilon_D = 4{\cdot}8 \times 10^{-15}$, and for the mass negligibility terms it leads to $\varepsilon_p = 4{\cdot}5 \times 10^{-12}$. So, both terms are effectively negligible compared to 1.

3.3.2. *Plate shape and pressure jump*

In this section, the plate displacement $\bar{W}(x, y)$ and the pressure jump $\bar{P}(x, y)$ relative to the case studied in the previous section are presented using $k_{max(mec)} = 168\ \mathrm{m}^{-1}$ and $k_{max(acou)}112 = \mathrm{m}^{-1}$. It is verified that the use of ectoplasm effectively cancels the pressure jump and permits large velocity magnitudes in the hole area.

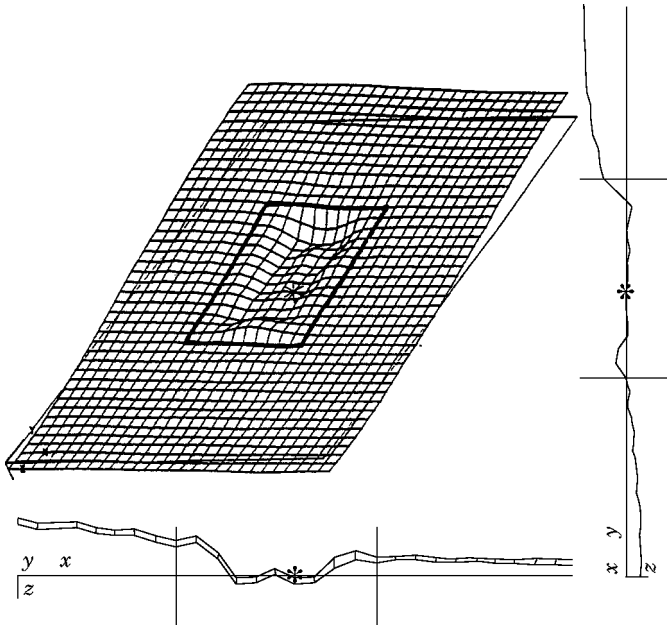

Figure 4. Real part of the pressure jump; the right side view represents the pressure jump along the axis $x = a/2$. The bottom side view represents the pressure jump along the axis $y = b/2$. Side views are given to show that the pressure jump tends toward zero in the hole surface.

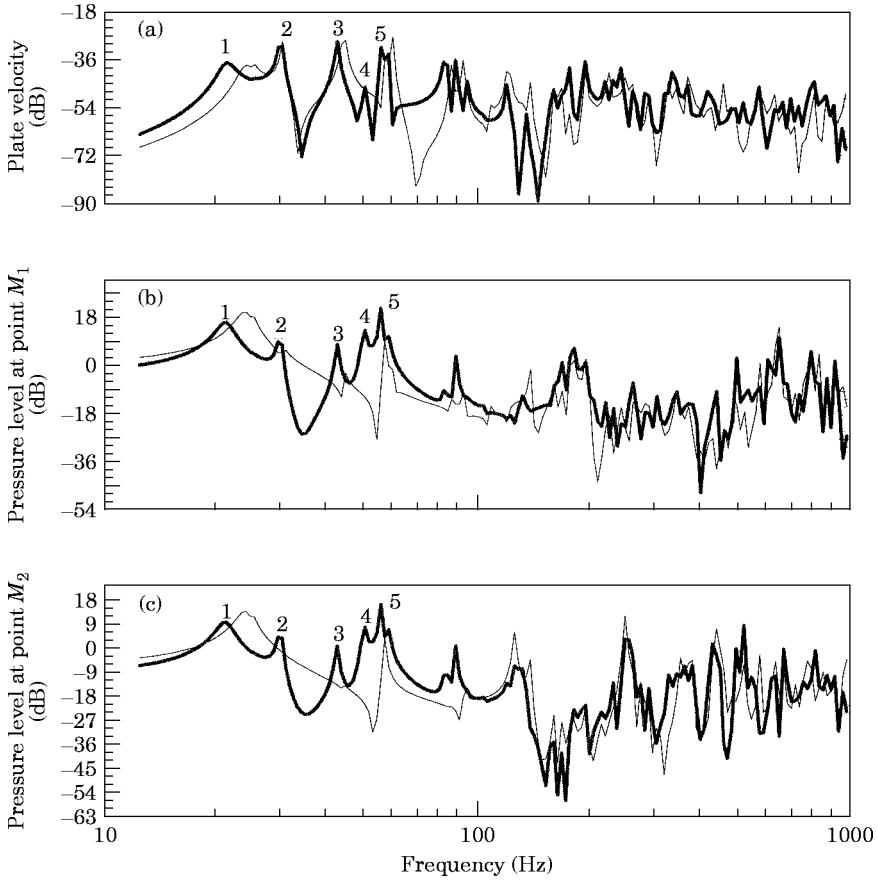

Figure 5. Simulation of the radiation of a full (thin line) and a holed (thick line) plate: (a) plate velocity, (b) acoustic pressure in the first cavity $z < z_p$, (c) acoustic pressure in the second cavity $z > z_p$.

In Figure 3(a), the holed plate displacement is represented on the S_p area only. In Figure 3(b), the plate displacement is represented on all of the domain S (including the hole area). The holed plate surface seems to be motionless in Figure 3(b). This is due to limited dynamics of graphical representation; velocities magnitudes in the hole area are one hundred times larger than those in the plate area. In Figure 4, the pressure jump is represented on all of the domain S. It can be seen that the pressure jump magnitudes in the hole area tend actually toward zero.

TABLE 2

Holed plate eigenfrequencies

Mode	1	2	3	4	5
Holed plate eigenfrequencies (Hz)	14·6	30·3	42·8	55·1	58·7
Full plate eigenfrequencies (Hz)	15·0	30·7	44·5	56·8	60·2

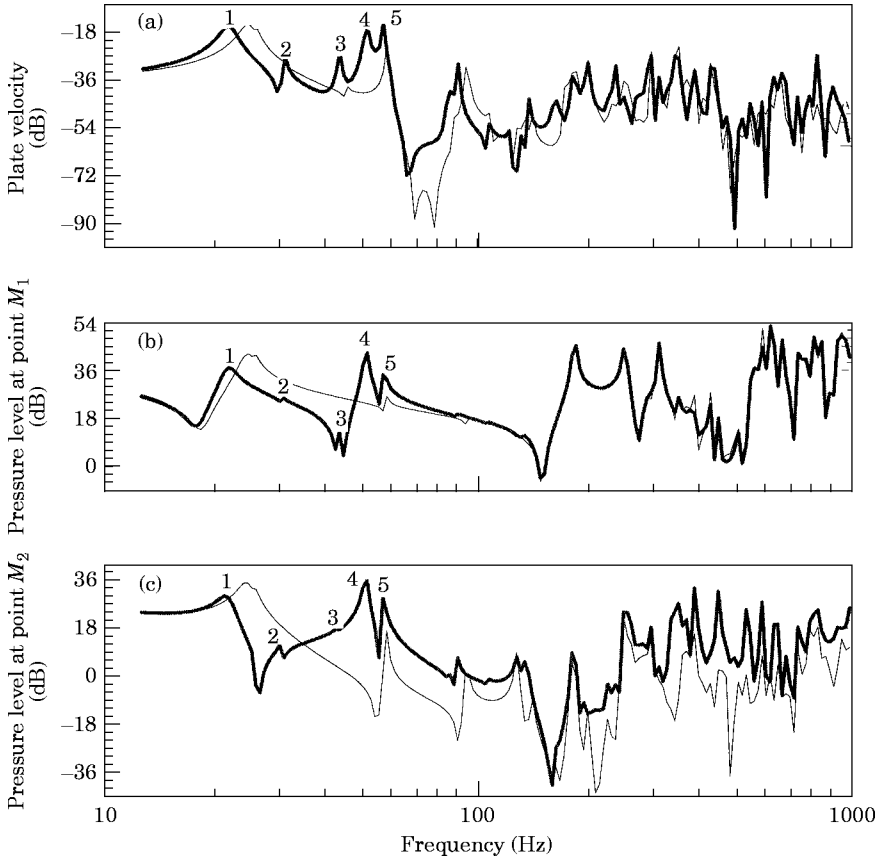

Figure 6. Simulation of the transmission loss of a full (thin line) and a holed (thick line) plate: (a) plate velocity, (b) acoustic pressure in the first cavity $z < z_p$, (c) acoustic pressure in the second cavity $z > z_p$.

4. ANALYSIS AND VALIDATION

In order to validate the developed numerical code, an experimental system was built to obtain measured data. The experimental set-up is described and theory/experiment comparisons are made, treating the cases of a holed plate and a full plate.

4.1. EXPERIMENTAL SETTING

The cavity was built with 22 mm thick plywood panels, except for one wall which was made of 20 mm thick plexiglas, that allowed visual control of microphones positions in the cavity. The interior cavity dimensions were $a = 0{\cdot}7$ m, $b = 1{\cdot}0\,m$, $l = 2{\cdot}0$ m. The relative lightness of such a set-up leads to non-negligible transmission losses of the walls at very low frequency (<30 Hz). However, this "low-cost" setting allowed essential tendencies to be obtained and to validate the numerical code. A 2 mm thick steel plate was placed at $z_p = 0{\cdot}6$ m. Such a plate thickness was retained in order to avoid losses through the plate boundaries, as cavity walls were not infinitely rigid. The acoustical source was a square loudspeaker (of size 10 cm) with a flat diaphragm where normal velocity is measured with a small accelerometer. A two channel analyser was used to generate white noise and to compute the transfer function between microphone (or accelerometer on the plate) and loudspeaker accelerometer (for transmission loss) or shaker force transducer (for radiation) (see equation (94) for the definition of the transfer function). Cavity and

plate damping were measured using the classical time decay method. Results are reported in Table 1. Pressure was measured on both sides of the plate at M_1(0·15, 0·70, 0·0.31) and M_2(0·20, 0·47, 1·42). An accelerometer was placed on the full or holed plate at co-ordinates (0·20, 0·56). The co-ordinates of the square loudspeaker centre were (0·51, 0·73). The shaker co-ordinates on the plate were (0·48, 0·25).

4.2. SIMULATION OF A FULL AND A HOLED PLATE

4.2.1. *General remarks*

In Figure 5, the simulation of a holed and a full plate radiation are compared. In Figure 6 the simulation of a holed and a full plate transmission loss are compared. Each time, the holed plate is presented with a thick line while the full plate is presented with a thin line. In this section, some general remarks about these curves are made.

The first cavity mode (excluding the Helmholtz mode) relative to the l-dimension of the cavity has an eigenfrequency of 87 Hz, so all the resonances below 87 Hz are only due to the plate. This acoustical mode is not clearly seen here as the plate is inserted in the cavity. However, the second cavity mode, at 173 Hz, relative to the b-dimension appears clearly with a small frequency shift due to the coupling between the plate and the cavity.

Eigenfrequencies of the first five in vacuo modes of a full and a holed plate are reported in Table 2, it can be seen that the hole has not a strong influence on the first five

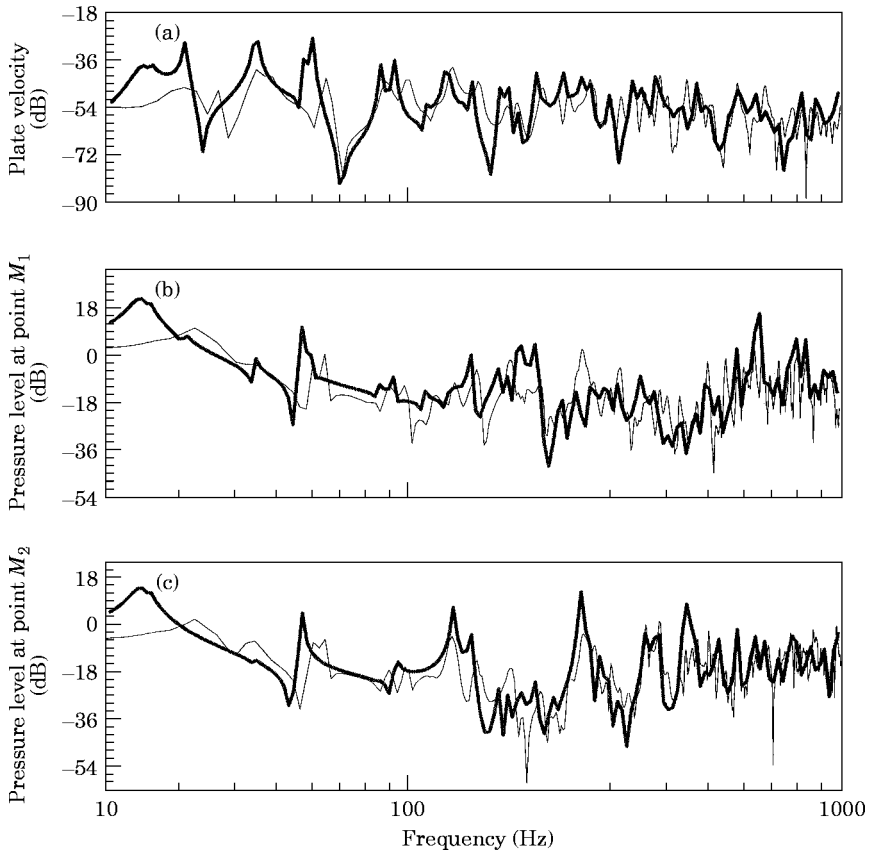

Figure 7. Radiation of a full plate; comparison of theory (thick line) with experiment (thin line): (a) plate velocity, (b) acoustic pressure in the first cavity $z < z_p$, (c) acoustic pressure in the second cavity $z > z_p$.

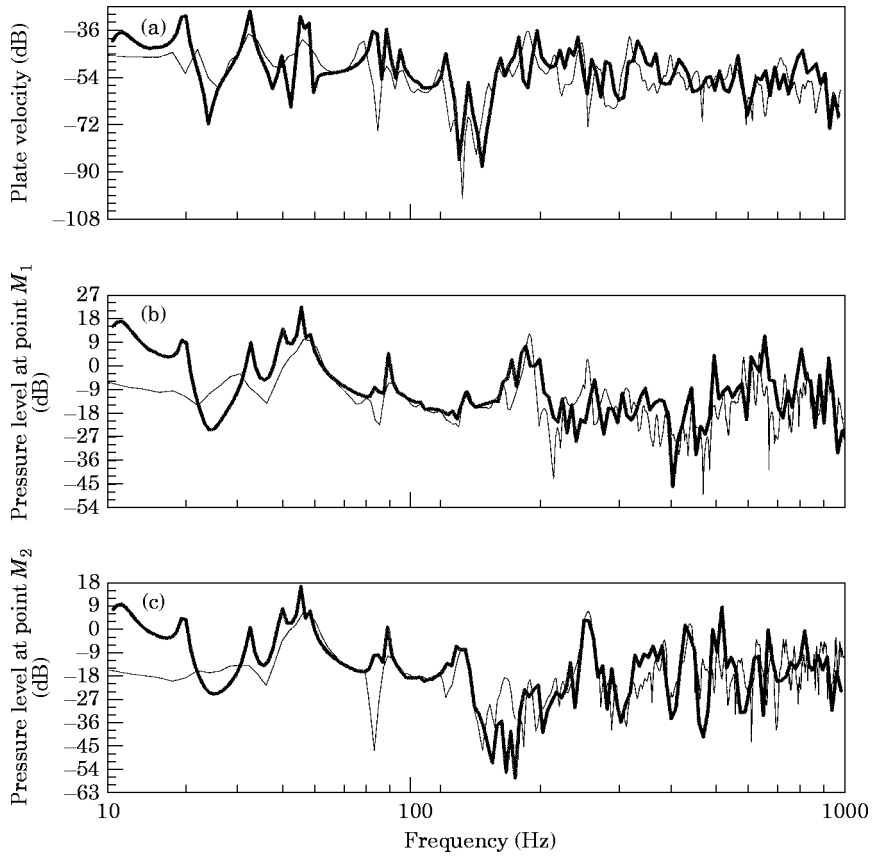

Figure 8. Radiation of a holed plate; comparison of theory (thick line) with experiment (thin line): (a) plate velocity, (b) acoustic pressure in the first cavity $z < z_p$, (c) acoustic pressure in the second cavity $z > z_p$.

eigenfrequencies. When the plate (full or holed) is coupled to the cavity, it can be seen in Figures 5(a) and 6(a) that some shifts appear at the plate resonances. Particularly, the first full plate mode is shifted by 6 Hz toward the higher frequencies. Such a shift was expected as it is well known that in this configuration only the Helmholtz mode is efficient; then, cavities act on the plate as additional stiffnesses. This effect of additional stiffnesses is still effective with a holed plate, but in a lesser way, as the hole allows a fluid transfer between the two parts of the cavity (short-circuit effect).

4.2.2. *Radiation of a full and a holed plate*

In this section, the influence of a hole on the plate radiation is discussed (Figure 5). It can be observed in Figure 5(a) that the first full and holed plate modes have almost the same vibration level, however, as can be seen in Figures 5(b) and 5(c), the first full plate mode, generate, higher pressure levels in both cavities than the first holed plate mode. As expected, the hole induces a short-circuit effect. The first mode radiation impedance is then decreased when the plate is cut out. Looking at Figure 5(a), it can be seen that the main effect of the hole on the plate vibration field is to shift eigenfrequencies, but most often the vibration levels remain similar at the plate resonances. Looking at Figures 5(b) and 5(c), it can be observed that the even full plate modes like modes 2 and 3 are non-radiative, while the corresponding holed plate modes are radiative. Actually, the plate symmetry is

broken when cutting out the plate; the mean value of the plate displacement is no longer zero and the plate become radiative. A similar effect of increased radiation when perturbing symmetries have been described for plates [18, 19] and shells [20] with added masses.

In summary, it can be concluded that the main influence of a hole on a rectangular simply supported plate radiation is to strongly increase the radiation of modes that were initially even (before cutting the plate). However, at very low frequency, the hole contributes to an expected short-circuit, decreasing the plate radiation. But this last effect cannot balance the main effect of increase, so in theory, a holed plate is noisier than a full one. However, in practice, a more temperate effect has to expected. Actually, the very low radiation efficiency of even modes of the theoretical full plate is due to its perfect symmetry. For a real life plate, the symmetry is generally destroyed by various heterogeneities so that an additional hole will probably not induce a strong perturbation of radiation.

4.2.3. *Transmission loss of a full and a holed plate*

In this section, the influence of a hole on the plate transmission loss is discussed. In Figure 6(a) it can be seen that, in opposition to the mechanical excitation case, the hole has a strong influence on the plate vibration field when the plate is acoustically excited. Actually, as shown in the previous section, when the plate is cut out, it no longer has

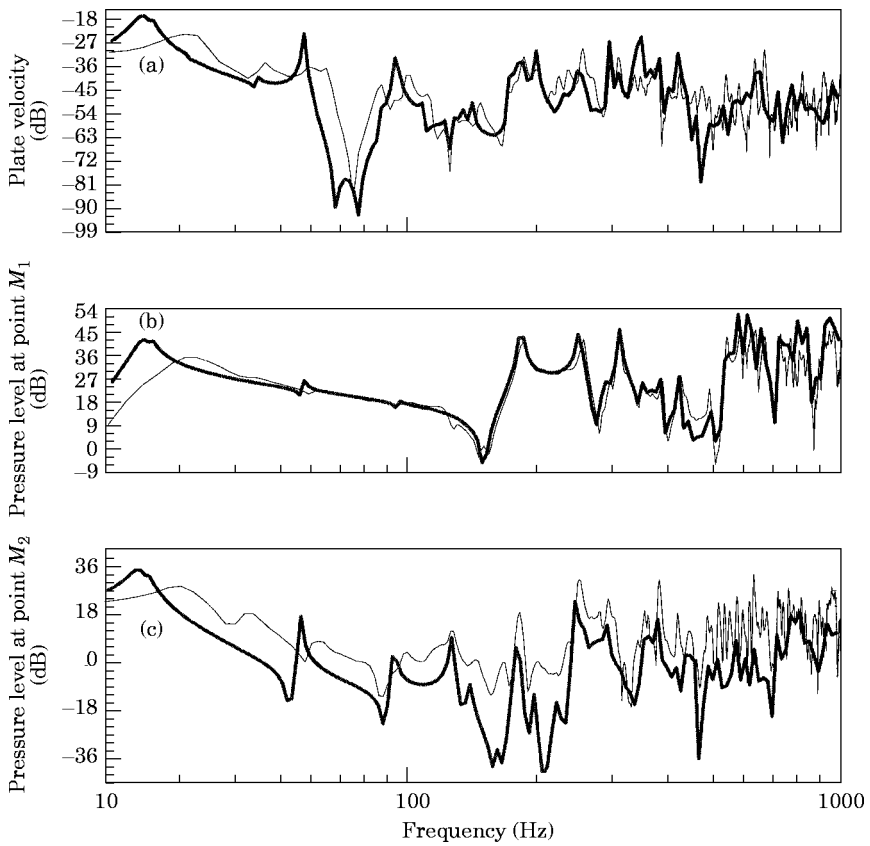

Figure 9. Transmission loss of a full plate; comparison of theory (thick line) with experiment (thin line): (a) plate velocity, (b) acoustic pressure in the first cavity $z < z_p$, (c) acoustic pressure in the second cavity $z > z_p$.

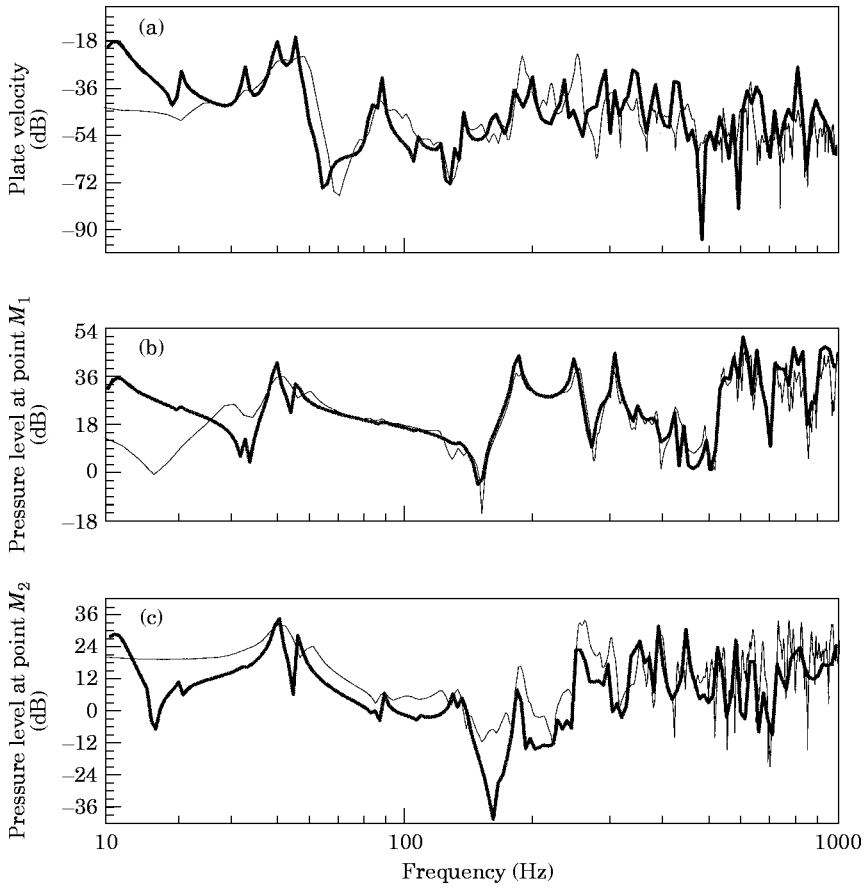

Figure 10. Transmission loss of a holed plate; comparison of theory (thick line) with experiment (thin line): (a) plate velocity, (b) acoustic pressure in the first cavity $z < z_p$, (c) acoustic pressure in the second cavity $z > z_p$.

symmetric modes so that all holed plate modes are coupled to the fluid medium. This is why, as shown in Figure 6(a), all holed plate modes are excited by the acoustical source. If a plate mode was initially antisymmetric (before cutting it out), the hole has almost no influence on the vibration level induced by the acoustical excitation at the mode eigenfrequency. For example, when considering mode 1 in Figure 6(a), it can be seen that the hole induces a frequency shift of the mode natural frequency; however, the plate velocity level remains the same. In contrast, if the mode was initially symmetric, then the hole has a great influence on the plate velocity level at the mode natural frequency because

TABLE 3

Free plate eigenfrequencies

Mode	Rigid body translation (Oz)	Rigid body rotation (Ox)	Rigid body rotation (Oy)	1	2	3	4	5
Free plate eigenfrequencies (Hz)	0·0	0·0	0·0	21·3	23·2	52·1	59·1	67·4
Simply supported plate eigenfrequencies (Hz)	–	–	–	15·0	30·7	44·5	56·8	60·2

such a mode is turned into a non-symmetric, and therefore acoustically excitable mode when a hole is cut out (for example, see modes 2 and 3 in Figure 6(a)).

Figure 6(b) represents the transfer function between the normal velocity of the acoustical source and the acoustic pressure at point M_1 situated at co-ordinates $x_1 = 32{\cdot}5$ cm, $y_1 = 50$ cm, $z_1 = 55$ cm in the cavity containing the acoustic source. Above 100 Hz, the presence of the hole has no influence on the pressure, the pressure field being dominated by the acoustic source and the geometry of the first cavity ($z < z_p$); the part of the pressure radiated by the plate is negligible. However, under 100 Hz, the presence of the hole has a strong influence on the pressure field, and acoustic pressure peaks can be found at holed plate resonances, so in this low frequency band, the radiation of the plate in the first cavity is not negligible.

Figure 6(c) represents the transfer function between the normal velocity of the acoustical source and the acoustic pressure at point M_2 situated at co-ordinates $x_2 = 32{\cdot}5$ cm, $y_2 = 50$ cm, $z_2 = 150$ cm in the cavity which does not contain the acoustic source. It is clear that, as expected, the holed plate has a lower insertion loss than a full plate as there is no obstacle to the acoustic field in the surface of the hole. Moreover, at low frequency (under 100 Hz) it can be seen that the holed plate vibration resonances can generate high pressure levels (see mode 4 and 5 resonances in Figure 6(c)). These holed plate vibration resonances contribute to a decrease of the insertion loss.

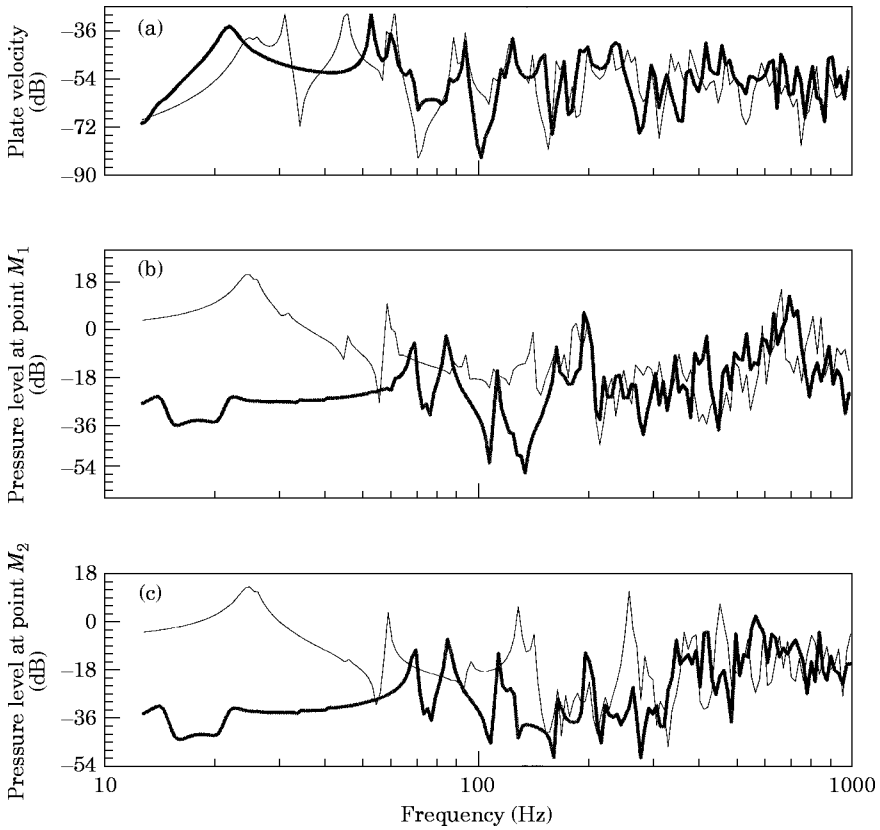

Figure 11. Simulation of the radiation of the unbaffled free plate (thick line) in comparison with the full plate (thin line): (a) plate velocity, (b) acoustic pressure in the first cavity $z < z_p$, (c) acoustic pressure in the second cavity $z > z_p$.

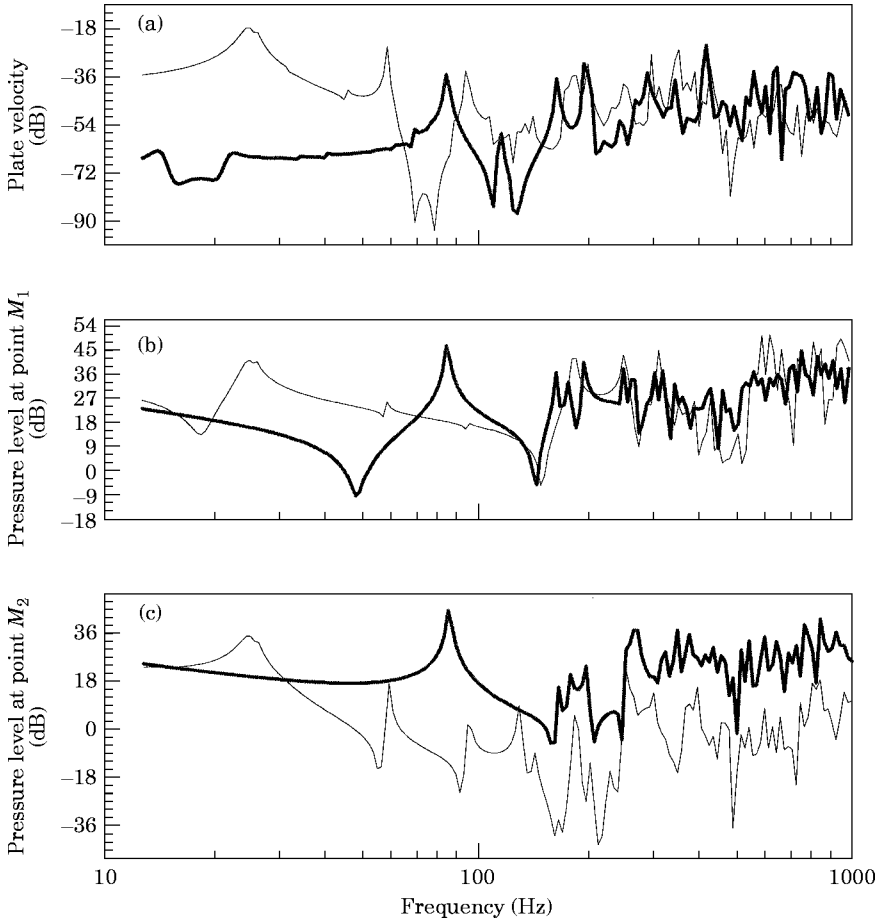

Figure 12. Simulation of the transmission loss of the unbaffled free plate (thick line) in comparison with the full plate (thin line): (a) plate velocity, (b) acoustic pressure in the first cavity $z < z_p$, (c) acoustic pressure in the second cavity $z > z_p$.

For transmission loss it can be concluded that the main tendency of a holed plate is to have a lower transmission loss than a full plate. This tendency was of course expected as diffraction through a hole is well understood. However, a supplementary and less expected reason is that a holed plate has less symmetries than a full plate (in the general case), causing it to be more strongly coupled with the fluid medium.

4.3. COMPARISON OF SIMULATION AND EXPERIMENT

Theoretical experimental comparisons for the radiation of holed and full plates are presented in Figures 7 and 8, respectively. Comparisons of the transmission loss of holed and full plates are presented in Figure 9 and 10, respectively. Measurements are presented by thin lines, while simulations are presented using thick lines. Simulations and experiments are in good agreement except at very low frequency (<30 Hz). This descrepancy at very low frequency was expected, because of the lightness of the experimental set-up. Flanking transmission through the walls was not negligible, moreover, the cavity was not perfectly airtight, so the Helmholtz mode (theoretically the only effective mode in this frequency range) could not pressurise the cavity as well as in theory. Another reason for discrepancy at very low frequency is the difficulty of producing

simply supported boundary conditions. In the frequency range of main interest, the theorical experimental agreement is very good, both in tendency and levels. It is uncommon to observe such a good validation when predicting this kind of phenomenon, resulting from cavity and structure coupling, both having multi-modal behaviour. This is true with a mechanical as well as with an acoustical excitation. Finally, to emphasise the validation of the method, it must be noted that this comparison is severe, as it is not based on global factors like radiation factor or mean squared pressure in the cavity, but on local data such as pressure or velocity at one particular point (even in the near field of the plate or of the source).

5. SIMULATION OF THE NON-BAFFLED FREE PLATE

Finally, in order to show what extreme cases can be treated using ectoplasm, the simulation of a non-baffled free plate in a cavity is presented and compared with a full plate in terms of radiation and transmission loss.

5.1. PRESENTATION OF THE NON-BAFFLED FREE PLATE

Geometrical and mechanical characteristics of this coupled system are the same as those presented in Section 4, except for the shape of the holed plate and the position of the mechanical excitation on the holed plate. The non-baffled free plate is simulated using a simply supported full plate of dimension $a = 0{\cdot}70$ m, $b = 1{\cdot}0$ m. A strip of 15 cm width is then cut out, around the full plate. A new smaller rectangular plate is then created of dimension $a' = 0{\cdot}40$ m, $b' = 0{\cdot}70$ m, having free edges. The first eight eigenfrequencies of this new free plate are presented in Table 3. (These *in vacuo* eigenfrequencies were calculated using a numerical code presented in reference [13]). The new position of the mechanical excitation on the non-baffled plate is $M_F(0{\cdot}40,\ 0{\cdot}55)$ referenced with the $Oxyz$-frame presented in Figure 1. To simulate the non-baffled free plate with respect to criteria presented in section 3, 1194 mechanical basis functions and 405 acoustical basis functions were used. The running time was 12 minutes per frequency point on an IBM RS 600/320 h. The full plate presented in this section is the same as the one presented in section 4.

5.2. RADIATION OF THE NON-BAFFLED FREE PLATE

In Figure 11 the non-baffled free plate radiation is compared with a full plate radiation (mechanical excitation). The non-baffled free plate is presented with thick lines, while the full simply supported plate is presented with thin lines. Both plates have the same velocity level. However, the non-baffled free plate radiation is not quite efficient in the low-frequency range compared with a full plate. The low-radiation of the non-baffled free plate at low-frequency is due to two main reasons: firstly, even if it was baffled, it is well known, as shown by Berry [21], that a plate having free edges radiates considerably less than a simply supported plate as the average of the plate displacement is close to zero for all modes (except for the rigid body mode of translation). Secondly, the plate is non-baffled, so its corners cannot radiate as shown for the baffled plate (reference [22], p. 67), because there is an acoustical short-circuit at the edge of the non-baffled plate. At high frequency non-baffled and full plates tend to achieve the same behaviour.

5.3. TRANSMISSION LOSS OF THE NON-BAFFLED FREE PLATE

In Figure 12 the non-baffled free plate transmission loss is compared with a full simply supported plate transmission loss. The non-baffled free plate is presented with thick lines, while the full plate is presented with thin lines. Regarding velocity levels, it can be seen

that below the first cavity mode (at 87 Hz), the acoustical source is unable to excite the non-baffled free plate. This can be understood, citing reciprocity of the short circuit effect explained for radiation. It can be observed that, at low frequency, non-baffled plate resonances do not act on the pressure in the cavity. The radiation of the plate is then negligible compared with the diffraction through the holes. The cavity resonance at 87 Hz does not appear when a full plate is inserted in the cavity, but this is not the case with a non-baffled plate where the cavity resonance at 87 Hz can be clearly observed. By looking at pressure levels in the receiving cavity (Figure 12(c)), it can be concluded that, as expected, the non-baffled plate transmission loss is lower than the full plate. However, in this particular case, an exception must be made for a small frequency range near the first eigenfrequency of the full plate where the full plate transmission loss is lower than for the non-baffled plate.

6. CONCLUSION

The goal of this work has been to propose a method for predicting sound radiation and transmission loss of plates with holes in order to explain the influence of a hole on the plate vibroacoustic behaviour. The expansion of the Green function on double indexed functions proposed by Bruneau [14] has been used with success. It leads to a simpler numerical code and implicitly allows to be taken into account the pressure jump across the plate, unlike the modal expansions on the cavity modes which were proposed by Ouellet *et al*. [12].

The notion of ectoplasm developed for vibrations in a previous paper [13] has been extended successfully to a vibroacoustic problem. By prolonging the holed plate on a canonical domain instead of considering the initial complex plate surface, many simplifications occur in the semi-analytical calculus. Criteria about the negligibility of ectoplasm compared with the fluid medium impedance has been given in order to use it with good accuracy. Extreme cases of holes can be treated using ectoplasm without being worried with ill-conditioning problems, as illustrated with the case of the non-baffled free plate. This proposed method has been exploited to simulate the sound pressure radiated by a guitar [23], and it could probably be extended to numerical approaches in order to avoid ill-conditioned matrices.

The method has been validated by experiment using local data such as pressure or plate velocity at particular points and not only by global factors such as mean quadratic velocity or radiation factor.

Results obtained for a rectangular simply supported plate indicate certain physical tendencies. Cutting a hole in a plate makes the transmission loss worse and increases plate radiation, except for the first plate mode where the tendency is reversed. This singular behaviour of the first holed plate mode could be used and optimised for some targeted applications. If a hole is required in a noisy structure for non-acoustical reasons, the better way to modify the structure is to have regard for structural symmetries which preserve antisymmetrical modes and their interesting low radiation properties.

ACKNOWLEDGMENTS

The authors wish to acknowledge the support of the sponsor of this work, the French Ministry of Environment (Service de la Recherche et du Traitement de l'Information sur l'Environnement). The authors also wish to thank Professor J. Nicholas for numerous stimulating discussions.

REFERENCES

1. M. Salikuddin 1990 *Journal of Sound and Vibration* **139**, 361–381. Acoustic behaviour of orifice plates and perforated plates with reference to low frequency sound absorption.
2. M. Salikuddin and W. H. Brown 1990 *Journal of Sound and Vibration* **139**, 383–405. Non-linear effects in finite amplitude wave propagation through orifice plate and perforated plate terminations.
3. A. P. Dowling and I. J. Hughes 1992 *Journal of Sound and Vibration* **156**, 387–405. Sound absorption by a screen with a regular array of slits.
4. R. A. Pierri 1977 *M. Sc. Dissertation*, *University of Southampton*, *England*. Study of a dynamic absorber for reducing the vibration and noise radiation of plate-like structures.
5. M. S. Atwal and M. J. Crocker 1985 *Inter-noise* 85 *Proceedings*, *Munich*, *Germany*, 18–20 *Sept*. **I**, 389–392. The effect on the transmission loss of a double wall panel of perforating the second panel.
6. J. E. Ffowcs Williams 1972 *Journal of Fluid Mechanics* **51**, 737–749. The acoustics of turbulence near sound absorbent liners.
7. F. G. Leppington and H. Levine 1973 *Journal of Fluid Mechanics* **61**, 109–127. Reflexion and transmission at plane screen with periodically arranged circular or elliptical apertures.
8. F. G. Leppington 1990 *Proceedings of the Royal Society of London* **A 427**, 385–399. The effective boundary conditions for a perforated elastic sandwich panel in a compressible fluid.
9. J. Pan, C. H. Hansen and D. A. Bies 1992 *Journal of Sound and Vibration* **156**, 349–359. Use of perforated panels for the active control of sound radiated from vibrating structures, I: Low-frequency analysis.
10. F. P. Mechel 1986 *Acustica* **61**, 87–104. Schalldurchgang durch Löcher und Schlitze mit Absorberfüllung und Verseigelung (transmission of sound through holes and slits filled with absorber and sealed).
11. Y. Murashi, H. Ohkawa, H. Tachibana and M. Koyasu 1985 *Inter-noise* 85 *Proceedings*, *Muchich*, *Germany*, 18–20 *Sept*. **I**, 409–412. Sound transmission characteristics of small apertures situated in the wall of buildings.
12. D. Ouellet, J. L. Guyader and J. Nicolas 1991 *Journal of Acoustical Society of America* **89**, 2131–2139. Sound field in a rectangular cavity in the presence of a thin, flexible obstacle by the integral equation method.
13. O. Beslin and J. L. Guyader 1996 *Journal of Sound and Vibration* **191**, 935–954. The use of an ''Ectoplasm'' to predict free vibrations of plates with cut-outs.
14. M. Bruneau 1983 *Introduction aux théories de l'acoustique* (*Introduction to acoustic theories*). Université de Maine, Le Mans, France: p. 634.
15. A. D. Pierce 1981 *Acoustics*: *an Introduction to its Physical Principles and Applicatons*. New York: McGraw-Hill Company, p. 642.
16. J. Bass 1968 *Cours de Mathématiques*. (*Lessons of Mathematics*). Paris; Masson: third edition **1**, p. 685.
17. O. Beslin 1993 *Ph.D. Thesis submitted to Institut National des Sciences Appliquées de Lyon*, *Lyon*. Rayonnement et transparence acoustique des plaques trouées (radiation and transmission loss of holed plates) p. 208.
18. E. E. Watson 1974 *Journal of Sound and Vibration* **36**, 439–441. Holographic sound detection of a rectangular plate with a mass loading.
19. D. M. Donskoi, A. E. Ekimov and A. V. Lebedev 1988 *Soviet Physics-Acoustics* **34**, 362–364. Influence of a mass inhomogeneity on sound radiation from massive plates.
20. E. Rebillard, B. Laulagnet and J. L. Guyader 1992 *Journal of Applied Acoustics* **36**, 87–106. Influence of an embarked spring-mass system and defects on the acoustical radiation of a cylindrical shell.
21. A. Berry, J. L. Guyader and J. Nicolas 1991 *Journal of the Acoustical Society of America* **88**, 2792–2802. A general formulation for sound radiation from recangular baffled plates with arbitrary boundary conditions.
22. F. J. Fahy 1989 *Sound and Structural Vibration*. *Radiation*, *Transmission and Response*. London: Academic Press, p. 309.
23. T. Carter and J. L. Guyader 1994 *Journal of the Acoustical Society of America* **95**, Part 2, 2913. Synthesis of the sound pressure radiated by a guitar using a mixed time- and frequency-domain modeling technique.